Utilization of Faraday Mirror in Fiber Optic Current Sensors

Petr DREXLER, Pavel FIALA

Dept. of Theor. and Experimental El. Engg., Brno University of Technology, Kolejní 2, 612 00 Brno, Czech Republic

drexler@feec.vutbr.cz, fiala@feec.vutbr.cz

Abstract. *Fiber optic sensors dispose of some advantages in the field of electrical current and magnetic field measurement, like large bandwidth, linearity, light transmission possibilities. Unfortunately, they suffer from some parasitic phenomena. The crucial issue is the presence of induced and latent linear birefringence, which is imposed by the fiber manufacture imperfections as well as mechanical stress by fiber bending. In order to the linear birefringence compensation a promising method was chosen for pulsed current sensor design. The method employs orthogonal polarization conjugation by the back direction propagation of the light wave in the fiber. The Jones calculus analysis presents its propriety. An experimental fiber optic current sensor has been designed and realized. The advantage of the proposed method was proved considering to the sensitivity improvement.*

Keywords

Fiber optic sensor, magneto-optic effect, Faraday mirror, linear birefringence, circular birefringence.

1. Introduction

The development of magneto-optic sensors has brought some new opportunities in current and magnetic field measurement. The principle of magneto-optic effects is based on the interaction between magnetic field and the phenomenon of light refraction and reflection in transparent medium and on its surface [1]. Three basic magneto-optic effects are known - Cotton-Mouton effect, Kerr surface effect and Faraday effect [2].

The most important for current sensor application is Faraday magneto-optic effect. Faraday effect causes the electromagnetic wave polarization rotation due to the magnetic field intensity in transparent material. The basic properties of this effect are high linearity (in the case of paramagnetic and diamagnetic materials), temperature dependence and the dependence on the wavelength. The magnitude of the effect depends further on the magneto-optic material constant (Verdet constant) and on the interaction length through which the wave travels in magnetized material.

The property of magneto-optic material which has to be observed is the presence of linear birefringence and its rate to induced circular birefringence. Circular birefringence is induced by the magnetic field. By evaluating the rate of circular birefringence it is possible to determine the intensity of the magnetic field. The linear birefringence is an undesirable effect which affects the polarization state of the wave. Input linear polarization state is modified to the elliptically polarized one and the sensitivity of circular birefringence evaluation is rapidly decreased. The linear birefringence can be of a latent origin. It can be induced by outer mechanical and thermal impacts further. It is important to watch the possibility of linear birefringence induction in designed sensors and try to prevent it. In the case of some sensor fabrication it is not possible to satisfy this and the requirement of suppression or compensation occurs. Some methods for linear birefringence suppression based on diverse principles [3], [4] have been published. The most advantageous method is based on the compensation of a phase shift of the orthogonal wave components. This method utilizes orthoconjugation retroreflector which allows the back propagation of the wave with conjugated orthogonal components. The wave component which travels forward aligned with the fast axis travels back aligned with the slow axis. Equally, the forward traveling slow-axis component travels back as the fast-axis component. The phase shift which the wave components experienced is equalized. The output polarization state is rotated by the angle $\theta = 90°$ in respect to the input polarization state.

2. Faraday Magneto-Optic Effect

The Faraday magneto-optic effect induces the optical activity due to the material magnetization. We can observe this effect in lot of materials with crystallic and amorphous structure. The analysis of Faraday effect appears from the interaction of electric field intensity $\boldsymbol{E}$ of the wave and the electron kinetics. Electrons represent oscillators described by the equation of enforced oscillation of the undamped harmonic oscillator [5]. The influence of the magnetic field wave component is negligible due to its low intensity. In

the presence of outer magnetic field with the flux density $\boldsymbol{B}$ parallel to the wave propagation it is in force the equation

$$m_{\mathrm{e}} \frac{\mathrm{d}^2 \boldsymbol{r}}{\mathrm{d}t^2} + \kappa \boldsymbol{r} = -e\boldsymbol{E} - e\left[\frac{\mathrm{d}\boldsymbol{r}}{\mathrm{d}t} \times \boldsymbol{B}\right] \tag{1}$$

where m_{e} is the electron mass, e is the electron charge, $\boldsymbol{r}$ is the vector which determines the electron displacement, $\kappa\boldsymbol{r}$ is the quasi-elastic force preserving electron in equilibrium. Electric field of the wave polarizes the medium

$$\boldsymbol{P} = -N_{\mathrm{e}} e \boldsymbol{r} \tag{2}$$

where N_{e} is the count of electrons in volume unit which are deflected by the electric field. Substituting equation (2) into (1) we get

$$\frac{\mathrm{d}^2 \boldsymbol{P}}{\mathrm{d}t^2} + \frac{e}{m_{\mathrm{e}}}\left[\frac{\mathrm{d}\boldsymbol{P}}{\mathrm{d}t} \times \boldsymbol{B}\right] + \omega_0^2 \boldsymbol{P} = \frac{N_{\mathrm{e}} e^2}{m_{\mathrm{e}}} \boldsymbol{E} \tag{3}$$

where ω_0 is the eigenfrequency of the electron oscillator. Equation (3) represents the system of two simultaneous differential equations. We obtain two terms by their solution. One for the right-hand, the second for the left-hand circular polarized wave in the medium

$$E_{\mathrm{r}} = E_{\mathrm{r}0} e^{j\omega t}, \quad E_{\mathrm{l}} = E_{\mathrm{l}0} e^{j\omega t}. \tag{4}$$

The macroscopic relation for the medium polarization due to the electric field of circular polarized waves is in the form

$$P_{\mathrm{r}} = \varepsilon_0 \chi_{\mathrm{r}} E_{\mathrm{r}}, \quad P_{\mathrm{l}} = \varepsilon_0 \chi_{\mathrm{l}} E_{\mathrm{l}} \tag{5}$$

where χ_{r} and χ_{l} is the dielectric susceptibility for right-hand and left-hand circular polarized wave and ε_0 is the permittivity of vacuum. Refractive index of the medium is related to dielectric susceptibility

$$n^2 = \varepsilon_r = 1 + \chi. \tag{6}$$

Substituting equations (5) into system (3) and by the utilization of relation (6) we obtain the relations for refractive index of right-hand and left-hand circular polarized wave

$$\begin{aligned} n_{\mathrm{r}}^2 &= 1 + \frac{N_{\mathrm{e}} e^2}{\varepsilon_0 m_{\mathrm{e}}} \cdot \frac{1}{\omega_0^2 - \omega^2 + \dfrac{e}{m_{\mathrm{e}}} B\omega}, \\ n_{\mathrm{l}}^2 &= 1 + \frac{N_{\mathrm{e}} e^2}{\varepsilon_0 m_{\mathrm{e}}} \cdot \frac{1}{\omega_0^2 - \omega^2 - \dfrac{e}{m_{\mathrm{e}}} B\omega}. \end{aligned} \tag{7}$$

When we take into account certain simplifications [6] we can differentiate equations (7). Consider l as an interaction length and B as the magnetic flux density, the polarization rotation angle is

$$\theta = \frac{\pi}{\varepsilon_0 \lambda_0} \frac{N_{\mathrm{e}}}{n_{\mathrm{m}}} \frac{e^3}{m_{\mathrm{e}}^2} \frac{\omega}{\left(\omega_0^2 - \omega^2\right)^2} Bl = VBl = \mu VHl \tag{8}$$

where $n_{\mathrm{m}}=(n_{\mathrm{r}} + n_{\mathrm{l}})/2$ is the medium refractive index, V is the Verdet constant which determines magneto-optic properties of medium. It is obvious that Verdet constant depends on the wavelength.

Equation (8) is the basic relation for Faraday magneto-optic effect. The polarization rotation θ is directly proportional to magnetic flux density B in the interaction length l. The effect is non-reciprocal. The polarization rotation direction depends on the mutual orientation of magnetic flux density $\boldsymbol{B}$ and the propagation direction. The polarization of wave propagating in the direction of $\boldsymbol{B}$ experiences a rotation with an angle θ. The polarization of wave propagating in the opposite direction to $\boldsymbol{B}$ experiences a rotation with an angle $-\theta$.

3. Integral Magneto-Optic Sensor

For the current sensor realization it is advantageous to utilize the concept of integral fiber-optic sensor. Single mode optical fiber serves as a magneto-optic element, which is called Faraday rotator. The basic setup is shown in Fig. 1.

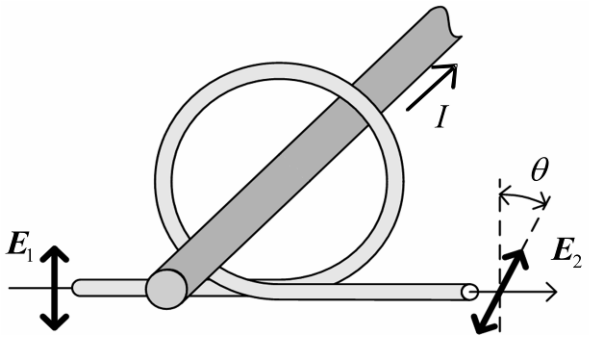

Fig. 1. The principle of integral fiber-optic current sensor.

The sensor principle is based on the Ampere's law

$$\oint_l \boldsymbol{B} \cdot d\boldsymbol{l} = \mu I \tag{9}$$

where μ is the permeability of Faraday rotator material. For diamagnetic and paramagnetic materials holds $\mu \cong \mu_0$ where μ_0 is the permeability of vacuum. Magnetic flux density vector $\boldsymbol{B}$ circulates round the conductor with the current. Faraday rotator in the form of loop of optical fiber encircles the conductor and implements the integration loop in (9). Only currents which are encircled by the integration loop contribute to the flux density $\boldsymbol{B}$. Further, the magnitude of integral (9) is not affected by the conductor position in the loop and does not depend on the integration loop length. The influence of currents outside the sensor is suppressed and it is not necessary to define the mutual position of the conductor and the sensor. The optical fiber can be wound with several loops around the conductor for improving sensitivity. It is possible to construct a sensitive sensor based on optical fiber with low Verdet constant. With respect to (8) and (9) we can derive the relation for

polarization rotation angle in fiber-optic sensor with number of loops N

$$\theta(t) = \mu V \oint_l \boldsymbol{B}(t) \cdot d\boldsymbol{l} = \mu_0 V N i(t) \cdot \tag{10}$$

For a given rotator with Verdet constant V the polarization rotation in time $\theta(t)$ depends only on the measured current waveform $i(t)$. The rate of the polarization rotation and the measured current value can be evaluated by means of polarimetry.

4. Linear Birefringence Suppression

Considering the need for preservation of single polarization state during the propagation the application of single mode fiber is demanded. The fiber core material (SiO_2) has a relatively low Verdet constant value $V = 3{,}67$ rad·T^{-1}·m^{-1}. However, it is possible to provide sufficient sensitivity with an adequate fiber loops count. Winding a fiber in loops leads unfortunately to mechanical stress and consecutively to linear birefringence formation in the fiber core. The linear polarization of coupled light wave transforms into elliptical polarization and sensor sensitivity is decreased. Consider a single mode fiber with diameter D_c which is wounded into a single loop with radius R_l. The specific phase shift δ_s which experience both orthogonal wave components is [7]

$$\delta_s = \frac{\pi}{\lambda} E_c C_c \frac{D_c^2}{4R_l^2} \tag{11}$$

where λ is the wavelength of the couple light wave, E_c is Young's modulus, C_c is the stress-optic coefficient. For silica fiber, $E_c = 7{,}45 \cdot 10^9$ Pa and $C_c = -3{,}34 \cdot 10^{-11}$ Pa^{-1} at $\lambda = 633$ nm [7].

Some methods for linear birefringence suppression based on diverse principles have been published. The basic method utilizes a twisted single mode fiber [3]. The twisting imposes a circular birefringence into a fiber. The rate of circular birefringence exceeds the rate of linear birefringence. A similar approach employs Spun HiBi fibers (Spun High Birefringence) [4]. In this type of fibers a chiral stress components are formed in the fiber cladding which impose a circular birefringence. In both approaches the linear birefringence can be neglected. The magneto-optic circular birefringence is superimposed to the latent one and its rate of change can be evaluated. The disadvantage of these methods is strong temperature dependence of the latent circular birefringence.

Another approach is fiber annealing [8]. A fiber coil is fixed in a ceramic labyrinth. This setup is exposed to annealing with a slow temperature rise in the range $10^{-1} \div 10^{0}$ °C/min. After the temperature achieves 800 °C, it is stabilized for several hours. Subsequently, the temperature is slowly decreased with steepness 0.1 °C/min. The influence of high temperature treatment reduces the inner mechanical stress in the fiber coil and the linear birefringence rate is decreased. The temperature dependence of residual linear birefringence is also reduced [8].

The sensors with back light propagation can be constructed for the birefringence compensation. This approach exploits the non-reciprocity of Faraday effect and the reciprocity of linear birefringence. The light wave is reflected on the far end and its polarization state is rotated with an angle $\theta = 90°$. Then, it is coupled back into the fiber. The light wave which travels the same path in the opposite direction experiences a double polarization rotation imposed by the Faraday effect, due to its non-reciprocity. The orthogonal wave components are swapped in relation to the fast and slow fiber axis (as described in the Introduction). The phase shift is equalized and the influence of linear birefringence disappears in the ideal case. In the real case the power losses in the fiber and by the light reflection lead to the presence of residual linear birefringence, which can decrease the sensitivity. The orthoconjugate retroreflector (OCR) is exploited for the light reflection and polarization rotation. The common term for this component is Faraday mirror, Fig. 2.

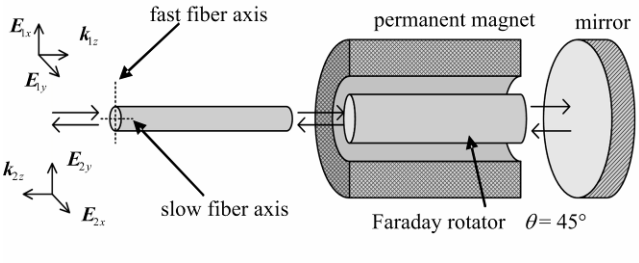

Fig. 2. The principle of orthoconjugate retroreflector (OCR).

In Fig. 2, after the orthogonal wave components $\boldsymbol{E}_{1x}$ and $\boldsymbol{E}_{1y}$ pass the optical fiber in forward direction, they experience a rotation $\theta = 45°$. When they are reflected by the mirror, they pass the Faraday rotator again. The resultant rotation is $\theta = 90°$. Now the orthogonal components pass the fiber back but in complementary fiber axis. We obtain a linearly polarized light on the close end of the fiber with the rotation $\theta = 90°$. When a magnetic field influences the fiber, the polarization will be different from the value $\theta = 90°$. This can be evaluated by means of polarimetry.

5. Theoretical Analysis of OCR

The Jones calculus can be exploited for theoretical analysis of fiber-optic sensor with OCR. The analyzed setup is shown in Fig. 3. For the simplification, following analysis does not take into account power losses in a fiber and on the optical components. In a real sensor, power losses are always present and they decrease its sensitivity. The next simplification is the assumption that the single mode fiber which is being analyzed is free from intrinsic linear birefringence. The linear birefringence is induced by

the fiber bending only. The experiments published in [9] show that this can be fulfilled for commercially available fibers. This allows to match the eigenstates to the coordinate systems which simplifies the analysis as shown below.

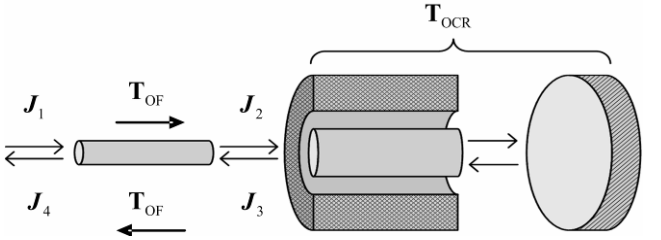

Fig. 3. The Jones calculus description of fiber optic sensor setup.

The light wave on the input of an optical fiber is described by the Jones vector $\boldsymbol{J}_1$. Consider the polarization angle $\theta = 45°$ compared to vertical. The light wave passes the fiber described by the matrix $\mathbf{T}_{\mathrm{OF}}$ and its polarization state is changed. The resultant vector is

$$\begin{aligned}\boldsymbol{J}_2 = \mathbf{T}_{\mathrm{OF}} \cdot \boldsymbol{J}_1 &= \frac{1}{\sqrt{2}}\begin{bmatrix} \alpha + \mathrm{j}\beta & -\gamma \\ \gamma & \alpha - \mathrm{j}\beta \end{bmatrix} \cdot \begin{bmatrix} 1 \\ 1 \end{bmatrix} = \\ &= \frac{1}{\sqrt{2}}\begin{bmatrix} \cos\Delta + \mathrm{j}\dfrac{\delta}{2}\dfrac{\sin\Delta}{\Delta} & -\phi\dfrac{\sin\Delta}{\Delta} \\ \phi\dfrac{\sin\Delta}{\Delta} & \cos\Delta - \mathrm{j}\dfrac{\delta}{2}\dfrac{\sin\Delta}{\Delta} \end{bmatrix} \cdot \begin{bmatrix} 1 \\ 1 \end{bmatrix} = \\ &= \frac{1}{\sqrt{2}}\begin{bmatrix} \alpha + \mathrm{j}\beta - \gamma \\ \alpha - \mathrm{j}\beta + \gamma \end{bmatrix},\end{aligned} \tag{12}$$

where

$$\Delta = \sqrt{\phi^2 + \left(\frac{\delta}{2}\right)^2} \tag{13}$$

is a geometric mean of phase shifts ϕ and δ which are imposed by the circular and unwanted linear birefringence [10].

The light wave $\boldsymbol{J}_2$ has generally elliptical polarization state and enters the OCR described by the matrix $\mathbf{T}_{\mathrm{OCR}}$. On the output we get

$$\begin{aligned}\boldsymbol{J}_3 = \mathbf{T}_{\mathrm{OCR}} \cdot \boldsymbol{J}_2 &= \frac{1}{\sqrt{2}}\begin{bmatrix} 0 & 1 \\ -1 & 0 \end{bmatrix} \cdot \begin{bmatrix} \alpha + \mathrm{j}\beta - \gamma \\ \alpha - \mathrm{j}\beta + \gamma \end{bmatrix} = \\ &= \frac{1}{\sqrt{2}}\begin{bmatrix} \alpha - \mathrm{j}\beta + \gamma \\ -\alpha - \mathrm{j}\beta + \gamma \end{bmatrix}.\end{aligned} \tag{14}$$

The light wave passes the fiber in the back direction and on its close end is described by the vector

$$\begin{aligned}\boldsymbol{J}_4 = \mathbf{T}_{\mathrm{OF}} \cdot \boldsymbol{J}_3 &= \frac{1}{\sqrt{2}}\begin{bmatrix} \alpha + \mathrm{j}\beta & -\gamma \\ \gamma & \alpha - \mathrm{j}\beta \end{bmatrix} \cdot \begin{bmatrix} \alpha - \mathrm{j}\beta + \gamma \\ -\alpha - \mathrm{j}\beta + \gamma \end{bmatrix} = \\ &= \frac{1}{\sqrt{2}}\begin{bmatrix} \alpha^2 + \beta^2 - \gamma^2 + 2\alpha\gamma + \mathrm{j}2\beta\gamma \\ -\alpha^2 - \beta^2 + \gamma^2 + 2\alpha\gamma - \mathrm{j}2\beta\gamma \end{bmatrix}\end{aligned} \tag{15}$$

The resultant vector (15) is relatively difficult to analyze regarding to the investigation of birefringence. For the solution of this challenge we can analyze the separate instances when only the linear or only the circular birefringence is present. The resultant polarization state is given by their superposition.

Consider the presence of linear birefringence δ only ($\phi = 0$). It is possible to modify the relation (12)

$$\begin{aligned}\boldsymbol{J}_2' = \mathbf{T}_{\mathrm{OF}} \cdot \boldsymbol{J}_1 &= \frac{1}{\sqrt{2}}\begin{bmatrix} \cos\dfrac{\delta}{2} + \mathrm{j}\sin\dfrac{\delta}{2} & 0 \\ 0 & \cos\dfrac{\delta}{2} - \mathrm{j}\sin\dfrac{\delta}{2} \end{bmatrix} \cdot \begin{bmatrix} 1 \\ 1 \end{bmatrix} \\ &= \frac{1}{\sqrt{2}}\begin{bmatrix} \alpha' + \mathrm{j}\beta' \\ \alpha' - \mathrm{j}\beta' \end{bmatrix}.\end{aligned} \tag{16}$$

After the back propagation in the fiber the light wave is described by the vector

$$\begin{aligned}\boldsymbol{J}_4' = \mathbf{T}_{\mathrm{OF}} \cdot \mathbf{T}_{\mathrm{OCR}} \cdot \boldsymbol{J}_2' &= \frac{1}{\sqrt{2}}\begin{bmatrix} \alpha' + \mathrm{j}\beta' & 0 \\ 0 & \alpha' - \mathrm{j}\beta' \end{bmatrix} \cdot \\ &\cdot \begin{bmatrix} \alpha' - \mathrm{j}\beta' \\ -\alpha' - \mathrm{j}\beta' \end{bmatrix} = \frac{1}{\sqrt{2}}\begin{bmatrix} \alpha'^2 + \beta'^2 \\ -\left(\alpha'^2 + \beta'^2\right) \end{bmatrix} = \\ &= \frac{1}{\sqrt{2}}\begin{bmatrix} \cos^2\dfrac{\delta}{2} + \sin^2\dfrac{\delta}{2} \\ -\left(\cos^2\dfrac{\delta}{2} + \sin^2\dfrac{\delta}{2}\right) \end{bmatrix} = \frac{1}{\sqrt{2}}\begin{bmatrix} 1 \\ -1 \end{bmatrix}\end{aligned} \tag{17}$$

It is obvious that we obtain a linearly polarized wave at the close end of the fiber. The polarization state is rotated with an angle $\theta = 90°$. The influence of linear birefringence has disappeared.

In the second instance, consider the presence of circular birefringence ϕ only ($\delta = 0$) which is induced by the measured magnetic field. The light wave at the far end of fiber is described by the vector

$$\begin{aligned}\boldsymbol{J}_2'' = \mathbf{T}_{\mathrm{OF}} \cdot \boldsymbol{J}_1 &= \frac{1}{\sqrt{2}}\begin{bmatrix} \cos\phi & -\sin\phi \\ \sin\phi & \cos\phi \end{bmatrix} \cdot \begin{bmatrix} 1 \\ 1 \end{bmatrix} = \\ &= \frac{1}{\sqrt{2}}\begin{bmatrix} \alpha'' & -\gamma'' \\ \gamma'' & \alpha'' \end{bmatrix} \cdot \begin{bmatrix} 1 \\ 1 \end{bmatrix} = \frac{1}{\sqrt{2}}\begin{bmatrix} \alpha'' - \gamma'' \\ \alpha'' + \gamma'' \end{bmatrix}\end{aligned} \tag{18}$$

After the back propagation in the fiber the light wave is described by the vector

$$\begin{aligned}\boldsymbol{J}_4'' = \mathbf{T}_{\mathrm{OF}} \cdot \mathbf{T}_{\mathrm{OCR}} \cdot \boldsymbol{J}_2'' &= \frac{1}{\sqrt{2}}\begin{bmatrix} \alpha'' & -\gamma'' \\ \gamma'' & \alpha'' \end{bmatrix} \cdot \begin{bmatrix} \alpha'' + \gamma'' \\ -\alpha'' + \gamma'' \end{bmatrix} = \\ &= \frac{1}{\sqrt{2}}\begin{bmatrix} \alpha''^2 - \gamma''^2 + 2\alpha''\gamma'' \\ -(\alpha''^2 - \gamma''^2 - 2\alpha''\gamma'') \end{bmatrix} = \\ &= \frac{1}{\sqrt{2}}\begin{bmatrix} \cos^2\phi - \sin^2\phi + 2\cos\phi\sin\phi \\ -\left(\cos^2\phi - \sin^2\phi - 2\cos\phi\sin\phi\right) \end{bmatrix} = \\ &= \frac{1}{\sqrt{2}}\begin{bmatrix} \cos^2\phi - \sin^2\phi + \sin 2\phi \\ -\left(\cos^2\phi - \sin^2\phi - \sin 2\phi\right) \end{bmatrix}.\end{aligned} \tag{19}$$

The term sin 2ϕ in (19) represents the phase shift due to the circular birefringence induced by the magnetic field. The light wave travels the fiber twice experiencing a double rotation 2ϕ. On the output of the fiber the polarization state can be evaluated by means of dual quadrature polarimetry. Both components of vector $\boldsymbol{J}_4$ can be detected in the channels with orthogonal polarizers (polarizing beam splitter). The components of Jones vector represent the electric field intensities. Optical power of the waves and the voltages on detector's output are proportional to the square of electric field intensities in both channels. The dependence of detected signal magnitudes on the rotation is shown in Fig. 4 for both orthogonal channels. We can find the characteristics linear for a small rotation angles.

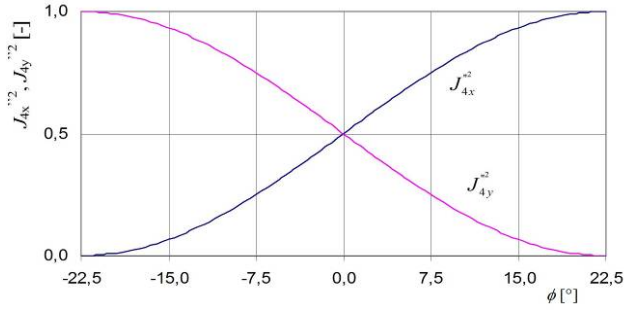

Fig. 4. The dependence of detected signal magnitudes on the polarization rotation.

6. Experimental Realization of Fiber Optic Sensor

On the base of obtained results in previous chapter a fiber optic current sensor has been designed. The sensor utilizes OCR in order to linear birefringence compensation. The scheme of the sensor is depicted in Fig. 5.

The source of the carrier optical signal is laser diode *L* with a single mode fiber pigtail. By the help of mating sleeve *S1* the fiber is connected to the second one with integrated collimator *C1*. The collimated beam is generally elliptically polarized. Polarizer *P* ensures initial linear polarization. After passing the non-polarizing beam splitter *NBS* the beam is coupled into the fiber via collimator *C2*.

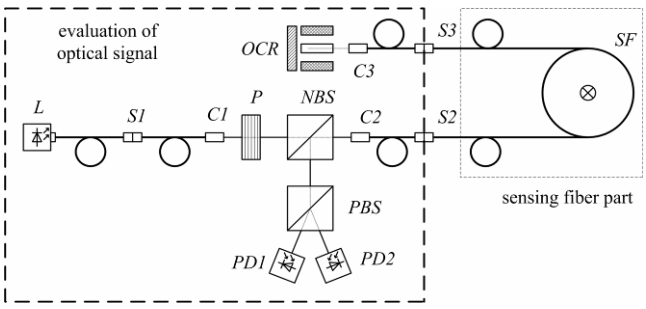

Fig. 5. The scheme of designed fiber optic current sensor.

The mating sleeves *S3*, *S2* join the sensing fiber part *SF* to the part of the optical signal evaluation. *C3* collimates the beam for OCR and couples it back into the fiber. After the back propagation, the divergent beam is collimated via *C2* and its part is deflected by means of *NBS*. The polarizing beam splitter *PBS* splits the beam in two orthogonal channels which are equipped with photodetectors *PD1* and *PD2*. *PBS* serves as a polarization analyzer. The whole sensor is designed for wavelength $\lambda = 633$ nm since silica fiber exhibits adequate magneto-optic sensitivity at this point. Standard single mode FC connectors were chosen. Polarizer *P* avoids the coupling of reflected beam back into the laser diode's pigtail, the power stability of the laser diode is not affected in this way.

The proposed sensor was experimentally realized for the pulsed current measurement in the range of kA. The value of Verdet constant limits theoretical maximal current value which is being measured. For the silica fiber with the core material constant $V = 3.67$ rad·T^{-1}·m^{-1} the maximal current value for one fiber loop $N = 1$ is

$$I_{\max} = \frac{\theta_{\max}}{\mu_0 V N} = \frac{\pi}{4 \cdot 4\pi \cdot 10^{-7} \cdot 3,67 \cdot 1} = 170 \text{ kA}. \qquad (20)$$

The period of analyzer *PBS* polarimetric function ends at this point. In the real sensor the residual linear birefringence caused by the power losses decreases the sensor sensitivity and the maximal current value will be higher. However, the rate of this effect is difficult to estimate. It will depend on the way how the fiber is led to the sensing fiber coil. The bandwidth restriction is placed by the magneto-optical as well as by the electronic part of the sensor. When we aim on the magneto-optical part we can see that the bandwidth is limited by the time of light propagation in the sensing fiber coil. Consider one fiber loop with the radius $R_l = 5$ cm, and the fiber refractive index $n_f = 1.5$. The maximum bandwidth of the magneto-optical part of the sensor is

$$BW = \frac{0,44c}{2\pi R_l n_f N} = \frac{0,44 \cdot 3 \cdot 10^8}{2\pi \cdot 5 \cdot 10^{-2} \cdot 1,5 \cdot 1} = 280 \text{ MHz}. \qquad (21)$$

For sensitivity comparison, the current pulse measurement without and with the presence of OCR were performed. The identical conditions were kept for both cases. Fig. 6 shows a scheme of the experimental setup for current measurement without OCR. The sensor setup utilizing OCR is depicted in Fig. 7. By the reason of more complicated optical components adjustment only absolute polarimetric method with single analyzer *A* and single photodetectors *PD* was realized for the OCR demonstration purposes.

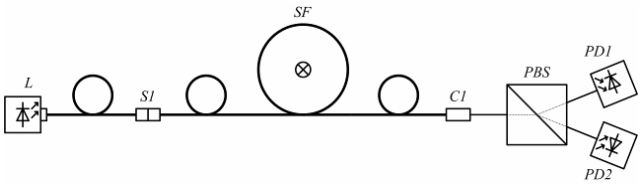

Fig. 6. The experimental sensor setup without OCR.

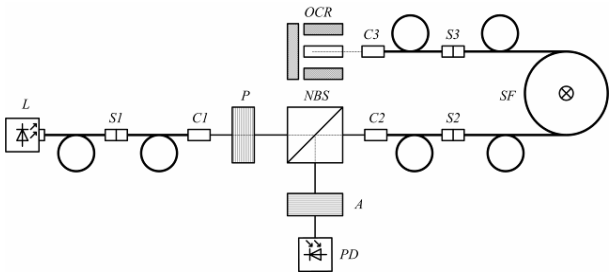

Fig. 7. The experimental sensor setup with OCR.

The experimental sensor setup employing OCR is shown in Fig. 8. For current generation a pulsed source with an inductive load was used [11]. The high voltage capacitor was discharged into a system of coils. The circuit was switched by the power thyristor module equipped with a control circuitry and fly-back diode. Two sensing fiber loops encircled two wire loops of the inductive load. A double current value was indicated then. The waveform of the current pulse was measured by the Rogowski coil sensor too. Since the output voltage of the Rogowski coil is proportional to the derivation of the current, it was integrated by means of the mathematical function of the oscilloscope. A pigtailed laser diode with operating wavelength $\lambda = 633$ nm and the power $P = 10$ mW was used as a laser source. The whole fiber optic part of the sensor employed a single mode fiber SM600 with cladding diameter $D_c = 125$ μm and core diameter $d_c = 4{,}3$ μm. Fig. 9 shows a detailed view of the OCR and the beam splitter with integrated fiber optic collimators.

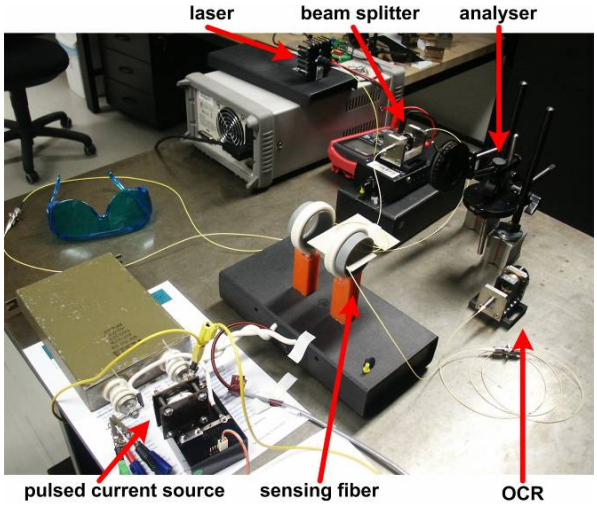

Fig. 8. The experimental setup of the magneto-optic current fiber sensor with OCR.

Fig. 9. The beam splitter assembly with polarizer and integrated collimators (left) and orthoconjugate retroreflector (right).

Resonant discharge circuit produced harmonic damped current waveform with oscillating frequency $f = 59$ kHz and first peak's value in the range of $I_p = 1300 \div 1600$ A. The current value was obtained by the help of a calibrated Rogowski coil sensor. Fig. 10 presents waveforms which were captured by the measurement without the OCR. Dual quadrature polarimetry using polarizing beam splitter and couple of photodetectors was used for optical signal evaluation [12]. The first waveform (from the top) in Fig. 10 is the Rogowski coil voltage and the second its integral, which indicates the real current waveform in the load with the top value $I_p = 1550$ A. The third and fourth waveforms are the voltages on the photodetector's outputs.

The waveforms which were captured by the current pulse measurement with OCR are shown in Fig. 11. The first waveform considered from the top is the Rogowski coil voltage. The second waveform is its integral, which represents the current waveform. The third waveform is the photodetector's output voltage. The duration of the current pulse, which is represented by the sinus half wave, was $t_d = 8.5$ μs and it reached the value up to $I_p = 1600$ A. It hasn't been able to achieve shorter pulses with this simple current generator. But the main goal of this experiment was to show the sensitivity improvement, not the bandwidth possibilities.

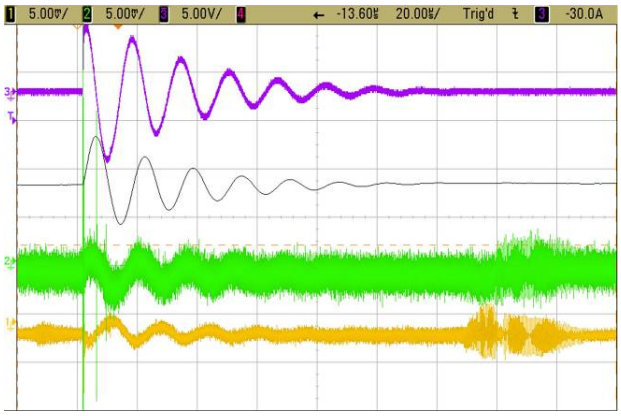

Fig. 10. The waveforms captured by the current pulse measurement without OCR.

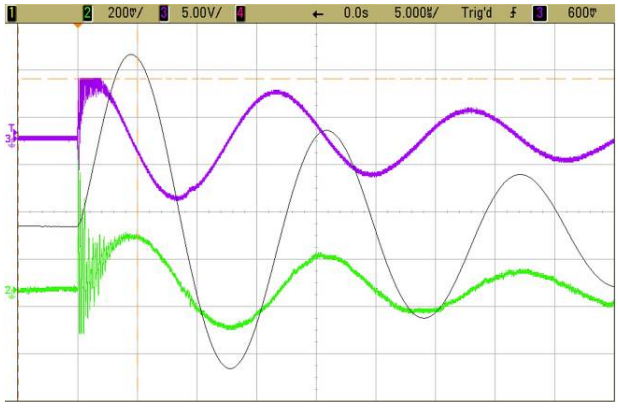

Fig. 11. The waveforms captured by the current pulse measurement with OCR.

When we compare the photodetector's output voltages in Fig. 10 and Fig. 11 it is obvious that only very low sensitivity was achieved with the sensor without OCR. In Fig. 10, the voltage value does not exceed 5 mV in the moment of the current top $I_p = 1550$ A.

The estimated voltage top value is $U_p = 1.4$ mV. A strong photodiode's shoot noise and thermal noise of the transimpedance amplifier dominates in the output signal. When the sensor with OCR was used for the current pulse measurement a much larger sensitivity was achieved, Fig. 11. The sensors output voltage $U_p = 214$ mV corresponds with the current top $I_p = 1365$ A. The sensitivity has improved by a factor $A_S = 174$. Interference is observable in the waveforms in Fig. 11. It is probably caused by the steep current rise by the thyristor switching.

7. Conclusion

The fiber optic sensors which have been described in this paper represents an advantageous way for DC and AC currents and magnetic fields measurement. Their advantages become significant by the measurement of pulsed quantities of very high level and very short time duration. The galvanic isolation is important in high voltage systems and prevents ground loops further. The carrier signal is a light wave which can be transmitted for a long distance without bandwidth limitation. The bandwidth is then determined mainly by the electronic part of the sensor.

The drawback of the single mode fiber optic sensors is the presence of latent and induced linear birefringence. It significantly reduces the sensor sensitivity due to the polarization state degeneration. However, some methods offer the suppression or compensation of the linear birefringence. In this work, the compensation method which utilizes orthogonal polarization conjugation has been chosen as a promising approach. It has been theoretically analyzed by means of Jones calculus. The ability of linear birefringence compensation has been proved together with double sensitivity improvement. The results of the analysis have been experimentally demonstrated by the measurement of the pulse current waveform.

Acknowledgements

The paper was prepared within the framework of the research plan No. MSM 0021630513 of the Ministry of Education, Youth and Sports of the Czech Republic.

References

[1] GAUGITSCH, M., HAUSER, H. Optimization of a magneto-optical light modulator. *Journal of Lightwave Technology,* 1999, vol. 17, no. 12, p. 2633 - 2644.

[2] CRAIG, A. E., CHANG, K. *Handbook of Optical Components and Engineering.* New Jersey: John Wiley & Sons, Inc., 2003.

[3] ROSE, A., REN, Z. F., DAY, G. W. Twisting and annealing optical fiber for current sensors. *Journal of Lightwave Technology*, 1996, vol. 14, no. 11, p. 2492 - 2498.

[4] LAMING, R. I., PAYNE, D. N. Electric current sensors employing spun highly birefringent optical fibers. *Journal of Lightwave Technology*, 1989, vol. 7, no. 12, p. 2084 - 2094.

[5] WAYNANT, R. *Electro-Optics Handbook*. New York: McGraw-Hill Professional, 2000.

[6] BORN, M., WOLF, E. *Principles of Optics.* Cambridge: Cambridge University Press, 1999.

[7] ULRICH, R., RASHLEIGH, S. C., EICKHOFF, W. Bending-induced birefringence in single-mode fibers. *Optical Letters*, 1980, vol. 5, p. 273 - 275.

[8] TANG, D., ROSE, A. H., DAY, G. W., ETZEL, S. M. Annealing of linear birefringence in single-mode fiber coils: Applications to optical fiber current sensors. *Journal of Lightwave Technology*, 1991, vol. 9, no. 8, p. 1031 - 1037.

[9] PAVLŮ, M. *The Suppression of Mechanical Stress Impacts in Fiber Optic Transmission Systems*. Bachelor's thesis. Brno: FEEC, Brno University of Technology, 2008.

[10] RIPKA, P. *Magnetic Sensors and Magnetometers.* London: IEEE; Artech House, 2001.

[11] DREXLER, P., FIALA, P. Methods for high-power EM pulse measurement. *IEEE Sensors J.*, 2007, vol. 7, no. 7, p. 1006 – 1011.

[12] DREXLER, P., FIALA, P. Identifying of the special purpose generator pulses. In *Proceedings of Progress in Electromagnetics International Conference PIERS 2007*. Beijing (China), 2007, p. 561 – 565.

About Authors...

Petr DREXLER graduated from the Faculty of Electrical Engineering and Communication, Brno University of Technology. Since 2004 he has been with the Department of Theoretical and Experimental Electrical Engineering, Brno University of Technology. He received Ph.D. degree in Electrical Engineering in 2007. He is interested in the domain of the electro/magnetooptical methods for electromagnetic field measurement, in the design of optoelectronic circuits and properties of electro/magnetooptical sensors. He is a member of the IEEE.

Pavel FIALA received Ph.D. in Electrical Engineering from the Brno University of Technology, Faculty of Electrical Engineering and Communication in 1998. He joined the Department of Theoretical and Experimental Electrical Engineering in 1990 as a research assistant. Since 2003 he has been Associate professor and head of the Department. Dr. Fiala is interested in modeling and analysis of coupled field problems by numerical method formulated with partial differential equations using the finite element method (FEM), the boundary element method and the finite difference method. In modeling and optimization, he introduced coupled electromagnetic-thermal-mechanical deformation of lumped parameters models. He is a co-director of the European project WISE – wireless sensing of the 6th framework dealing with sensor research for aeronautics and cosmonautics (participant consortium EADS, DASSAULT, AVIATION, etc.) and a member of the IEEE, IEE, OSA, APS, SPIE.